Synthesis of one-dimensional vanadium-doped CoS/Co_9S_8 heterojunctions as bifunctional electrocatalysts for zinc-air battery

Huiyong Huang [a], Anmin Liu [b, *], Qiaoling Kang [c], Xinyu Ye [a], Hanlin Chen [a], Wei-Nien Su [d], Tingli Ma [a, c, *]

[a] Graduate School of Life Science and Systems Engineering, Kyushu Institute of Technology, 2-4 Hibikino, Wakamatsu-ku, Kitakyushu, Fukuoka 808-0196, Japan

[b] State Key Laboratory of Fine Chemicals, School of Chemical Engineering, Dalian University of Technology, Panjin Campus, Panjin, 124221,

China.

[c] College of Materials and Chemistry, China Jiliang University, No. 258, Xueyuan Street, Xiasha Higher Education Zone, Hangzhou, Zhejiang, 310018, P. R. China.

[d] Graduate Institute of Applied Science and Technology, National Taiwan University of Science and Technology, Taipei, Taiwan.

Corresponding Authors

*E-mail: tinglima@life.kyutech.ac.jp

*E-mail: liuanmin@dlut.edu.cn

Abstract

Cobalt-based electrocatalysts have been considered promising materials for the oxygen evolution reaction (OER). Herein, we now report the synthesis of vanadium doped CoS/Co_9S_8 heterostructures embedded on carbon nanorods (V-CoS/Co_9S_8@CNR), which was realized through one-step sulfurization of Zeolitic Imidazolate Framework-67 (ZIF-67) grown on V_2O_5 nanorods (V_2O_5@ZIF-67). The results of experiment and

©2022. This manuscript version is made available under the CC-BY-NC-ND 4.0 license
http://creativecommons.org/licenses/by-nc-nd/4.0/

theoretical calculation verified that due to the vanadium dopant and the coupled nanointerface that can expedite the synergistic effect of Co_9S_8 and CoS, the obtained V-CoS/Co_9S_8@CNR showed an excellent OER catalytic performance (269 mV@10 mA cm^{-2}) and comparable ORR catalytic performance. The assembled rechargeable Zn-air batteries displayed a superior performance as well as high charging-discharging cycling stability (over 200 h) with a slight increase in the voltage gap.

KEYWORDS: CoS/Co_9S_8; Vanadium-doped; Electronic structure; One step; OER

1 Introduction

Rechargeable Zn-air batteries (ZABs) have recently drawn ongoing interest due to their fascinating merits, including non-toxicity, high theoretical energy density and sustainability [1, 2]. Unfortunately, the sluggish dynamics of the oxygen reduction reaction/oxygen evolution (ORR/OER) of the air cathode decrease the final energy output efficiency, which limits the commercialization of rechargeable ZABs [3-5]. Besides, the low storage capacity and unaffordable price of Pt and Ru/Ir oxides catalysts hamper their large-scale commercialization application in rechargeable ZABs [6-9]. Therefore, it is urgently required to rationally design and develop high-performance bifunctional OER and ORR electrocatalysts to facilitate the slow kinetics for the advanced ZABs.

Among the many noble-metal-free electrocatalysts for the OER, cobalt-based materials have been proven to be some of the most promising candidates due to their relatively cost-effective and reasonable activities for the OER [10-14]. The cobalt chalcogenides (such as $Co_{1-x}S$, CoS, Co_3S_4, Co_9S_8) have been considered as one kind of significant potential OER electrocatalyst [15-19]. However, the traditional preparation of cobalt sulfide includes two steps of the solvothermal reaction and calcination, which leads to excessive energy consumption. Therefore, it is necessary to develop a method to prepare cobalt sulfide in one step [20-24]. Recent studies have reported that the synergistic effect between composite catalysts and the introduction of foreign dopants can enhance the electrocatalytic performance of cobalt sulfide [25-32].

Herein, we now report a facile one-step sulfurization strategy to rationally design and synthesize vanadium doped CoS/Co_9S_8 heterostructures embedded onto carbon nanorods (denoted as V-CoS/Co_9S_8@CNR) as the OER and ORR electrocatalysts for ZABs in an alkaline medium. To the best of our knowledge, Co_9S_8-based heterostructures have been synthesized for OER research [19, 22, 27, 29], but this is the first example using composite catalysts of CoS/Co_9S_8 in the zinc-air battery. The synergetic effect between the two-phase interface can increase the surface area and conductivity of the sulfide phase, thereby significantly enhancing the electrochemical catalytic performance. Density functional theory (DFT) calculations proved that the vanadium dopant and the interface effect enhance the electron states around the Fermi level of V-CoS/Co_9S_8@CNR, indicating that the carrier density increases, which is beneficial to the electron transfer during the electrocatalytic process. As expected, when integrating the bifunctional ORR/OER electrocatalysts into the air electrode of the zinc-air battery, which exhibits up to 200 hours of cycle stability.

2. Experimental section

2.1 Synthesis of V_2O_5 nanowires

Typically, 0.6 gram of ammonium metavanadate and 1 gram of triblock copolymer (P-123) were dissolved in a solution of 0.1 M HCl (30 mL) with stirring for 7 h. Then, the mixed solution was transferred to a teflon-lined autoclave and heated at 120 °C for 24 h. After that, the yellowish product was separated by centrifugation with deionized water for several times.

2.2 Synthesis of ZIF-67

Typically, 1 mmol $Co(NO_3)_2 \cdot 6H_2O$ and 4 mmol 2-methylimidazole were dissolved in 100 mL methanol. After stirring for10 min, the mixtures were kept for 24 h at room temperature. Then the purple product was separated by centrifugation and washed thoroughly with methanol.

2.3 Synthesis of V_2O_5@ZIF-67

An amount of 25 mg as obtained V_2O_5 nanowires and 800 mg of PVP (Mw = 40,000) was well-dispersed in 40 mL of methanol under sonication condition; then, 291 mg of

$Co(NO_3)_2 \cdot 6H_2O$ and 328 mg of 2-Meththylimidazole was added to the above solution under continuous stirring. Two hours later, the purple solid product was separated by centrifugation with methanol three times and then dried at room temperature, which is called as V_2O_5@ZIF-67.

2.4 Synthesis of V-CoS/Co_9S_8@CNR

The as-prepared V_2O_5@ZIF-67 and L-cysteine were placed in a tune furnace, then pyrolyzed under an N_2 atmosphere at 500, 700, 900 °C with a heating rate of 5 °C min^{-1}, which are denoted as V-CoS@CNR, V-CoS/Co_9S_8@CNR, and V-Co_9S_8@CNR, respectively. For comparison, the synthetic procedure of CoS/Co_9S_8 was similar with that of V-CoS/Co_9S_8@CNR, except using ZIF-67 instead of V_2O_5@ZIF-67.

2.5 Details of theoretical calculation

The theoretical study of the density of states (DOS) for CoS, Co_9S_8, CoS/Co_9S_8, and V-CoS/Co_9S_8@CNR was carried out based on DFT using the CASTEP program in the Materials Studio package. In the Geometry Optimization and Single Point calculations, the PBE functional of GGA with Grimme method for the DFT-D correlation was utilized to describe the electronic exchange and correlation effects. Moreover, the plane-wave cutoff was tested and set to 500 eV. The self-consistent field tolerance was 2×10^{-6} eV with the OTFG ultrasoft pseudo-potential for core electrons.

3 Results and discussion

Scheme 1. Schematic of the preparation process of V-CoS/Co_9S_8@CNR.

The fabrication of V-CoS/Co_9S_8@CNR is illustrated in Scheme 1. First of all, we performed a facile process to obtain V_2O_5@ZIF-67 nanorods using solid V_2O_5 as templates in a methanol solution. The as-prepared V_2O_5@ZIF-67 and L-cysteine were then placed in the tube furnace and pyrolyzed under N_2 atmosphere. From the SEM image of V_2O_5, we can clearly see that the V_2O_5 shows a rod-like morphology and a smooth surface with a width of 50-100 nm (Figure 1a). After ZIF-67 was successfully assembled on the surface of V_2O_5, the surface of V_2O_5@ZIF-67 becomes rough (Figure 1b). Moreover, the TEM image clearly showed that the surface of V_2O_5 is completely covered by the rough ZIF-67 (Figure 1d). After thermal annealing at 700 °C, the morphology of the product does not significantly change (Figure 1c). When changing the thermal treatment temperature (500 and 900 °C), a similar nanorod structure can be retained, as shown in Figure S1 in the ESM. To further observe the internal structure, the magnified TEM image distinctly shows a distinct biphasic interface between CoS and Co_8S_9 in V-CoS/Co_9S_8@CNR, denoted by the red dashed line (Figure 1e), and the fringe spacing of 0.176 and 0.252 nm are related to the (440) plane of Co_9S_8 and (101) plane of CoS, respectively. As shown in Figure 1f, the images of the elemental mapping clearly show the simultaneous presence of the S, Co, V, C, O and N elements, which are evenly distributed on the surface of the V-CoS/Co_9S_8@CNR.

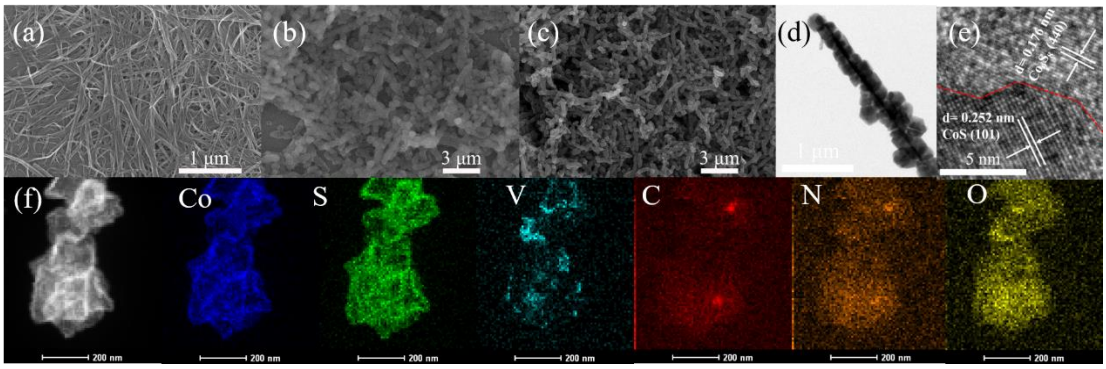

Figure 1. SEM images of V_2O_5 nanowire (a), V_2O_5@ZIF-67 (b) and V-CoS/Co_9S_8@CNR (c); (d) TEM images of V_2O_5@ZIF-67, (e) high resolution TEM images of V_2O_5@ZIF-67, (f) element mapping of V-CoS/Co_9S_8@CNR.

X-ray powder diffraction (XRD) was utilized to investigate the crystalline structures. The diffraction pattern of V_2O_5 matched the literature results [33] (Figure S3a in the

ESM). The diffraction pattern of V_2O_5@ZIF-67 in Figure S3a in the ESM matches the simulated XRD pattern of the ZIF-67 crystal. As shown in Figure 2(a), after thermal annealing at 700 °C, its diffraction peaks match well with the standard patterns of CoS and Co_9S_8. As shown in Figure 2b and Figure S4, the diffraction peaks of V-CoS/Co_9S_8 shifted slightly negatively to CoS/Co_9S_8, indicating that the unit cell structure of CoS/Co_9S_8 remained unchanged and an increased lattice distance after vanadium doping, which can be attributed to that Co^{3+} (0.545 Å, LS) is partially replaced by V^{4+} (0.580 Å). However, when the pyrolysis temperature is 500 or 900 °C, the diffraction peaks only match well with the standard pattern of CoS or Co_9S_8. The Raman peaks at around 463 and 665 cm^{-1} could be attributed to the characteristic peaks of Co_9S_8 [34, 35] (Figure 2c). The peaks at 1363 and 1588 cm^{-1} corresponded to the graphitic carbon structure (Figure S3c in the ESM). The vanadium oxide or nitride phase does not appear in XRD, which indicates that V was successfully doped instead of forming the V-based phase. These results are in well good great agreement with the XRD observation, further confirming the successful fabrication of the cobalt sulfide compound. Figure S5 shows that V-CoS/Co_9S_8@CNR has a typical mesoporous and microporous structure, indicating a typical mesoporous and microporous structure, which could provide more accessible catalytic sites and facilitate mass transport during the catalytic process.

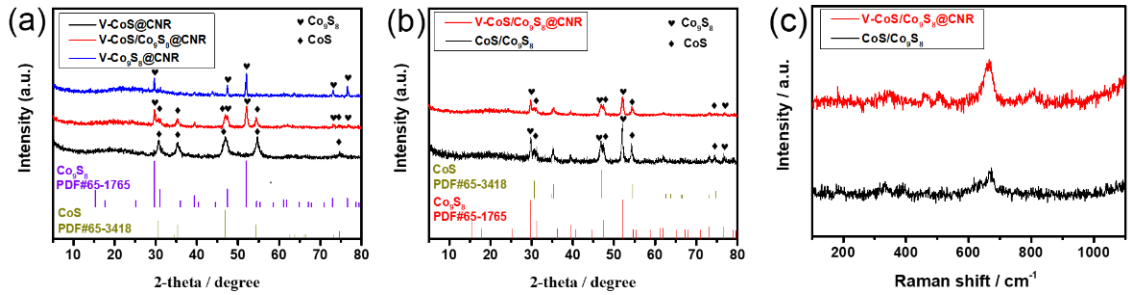

Figure 2. (a) XRD patterns of V-CoS@CNR, V-CoS/Co_9S_8@CNR and V-Co_9S_8@CNR; (b) Raman spectra of V-CoS/Co_9S_8@CNR and CoS/Co_9S_8, (c) Raman spectroscopy of V-CoS/Co_9S_8@CNR and CoS/Co_9S_8.

X-ray photoelectron spectroscopy (XPS) was used to further analyze the valence states and element compositions. As shown in Figure 3a, all elements (Co, O, V, N, C, S) are on the surface of V-CoS/Co_9S_8@CNR. Compared to the pure CoS/Co_9S_8, the XPS of Co 2p for V-CoS/Co_9S_8@CNR is positively shifted (Figure 3b), indicating that

vanadium effectively modulates its electronic state [20, 36]. The peak of S 2p of V-CoS/Co_9S_8@CNR is negatively shifted (Figure 3c), indicating that the S species in V-CoS/Co_9S_8@CNR have more partial negative charge of $S^{\delta-}$ than that in CoS/Co_9S_8 [20, 37-39]. The fitted peaks of V in V-CoS/Co_9S_8@CNR are high-valence $V^{4+}$and V^{5+} (Figure S6), which could provide plenty of vacant d-orbitals rendering a strong electrostatic attraction, as evidenced by the positive shifting of the Co 2p peaks compared to that of CoS/Co_9S_8 (Figure 3b).

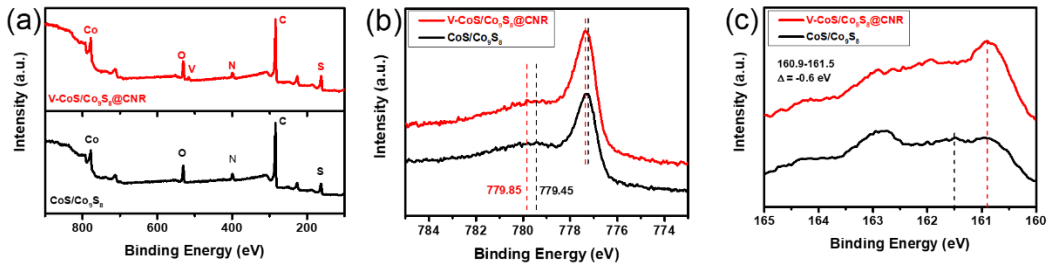

Figure 3. (a) XPS survey spectra, (b) Co 2p XPS spectra and (c) S 2p XPS spectra of V-CoS/Co_9S_8@CNR and CoS/Co_9S_8.

We then evaluated the OER activities of the obtained catalysts in a 1.0 M KOH solution by uniformly loading the homogenous ink on the hydrophobic carbon paper. The total catalyst loading is calculated to be about 2 mg cm^{-2}, close to the values in previous studies [25, 28, 40-43], the grid on the carbon paper in favor of stripping a generated bubble away from the electrode surface. As shown in Fig. 4(a), the OER performance of V-CoS/Co_9S_8@CNR is superior to RuO_2. Meanwhile, the Tafel plot value of V-CoS/Co_9S_8@CNR (67.2 mV dec^{-1}) is smaller than CoS/Co_9S_8 (98.1 mV dec^{-1}), and RuO_2 (85.3 mV dec^{-1}) (Fig. 4b, c). The smaller Tafel slope indicates a rapid increase in the O_2 generation rate with the applied overpotential, following the polarization curves. Moreover, the polarization curve of V-CoS/Co_9S_8@CNR after 1000 CV cycles (Fig. 4d) verified the high OER stability, indicating the apparent advantage of V-CoS/Co_9S_8@CNR as a high-performance OER electrocatalyst. In order to understand the high OER performance of V-CoS/Co_9S_8@CNR, we tested the Nyquist curve of different samples (Figure S7), V-CoS/Co_9S_8@CNR has a lower charge transfer than other samples, suggesting its faster charge transport kinetics. Besides, the electrochemically active surface area (ECSA) of all samples was evaluated by

measuring the electrical double-layer capacitance (C_{dl}). Figure S8 shows that V-CoS/Co_9S_8@CNR has the highest value (60.5 mF cm^{-2}), much larger than CoS/Co_9S_8 (28.1 mF cm^{-2}), V-Co_9S_8@CNR (16.5 mF cm^{-2}), V-CoS@CNR (10.5 mF cm^{-2}) and RuO_2 (5.4 mF cm^{-2}), confirming the largest ECSA of V-CoS/Co_9S_8@CNR. We also explored the effect of different calcination temperatures on the material. Figure S9a-c shows that changing the pyrolysis temperature will obtain different catalysts, and V-CoS/Co_9S_8@CNR shows the best catalytic performance. In addition to testing OER performance, we also the tested ORR performance (Figure S9d), Figure S9e shows that the electron transfer number of V-CoS/Co_9S_8@CNR is above 3.76, close to 4, proving that the ORR process is mainly four-electron pathway. Moreover, V-CoS/Co_9S_8@CNR shows good stability for ORR performance (Figure S9f). The above test results prove that the V-CoS/Co_9S_8@CNR catalyst we prepared has the promising potential for application in apply ZABs.

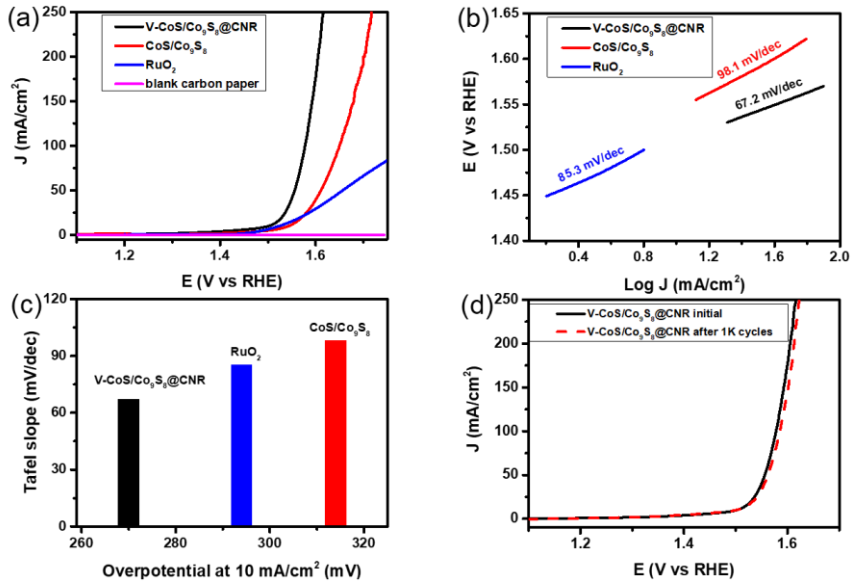

Figure 4. (a) Linear sweep voltammetry (LSV) curves for the OER of the V-CoS/Co_9S_8@CNR, CoS/Co_9S_8, and RuO_2 measured in O_2 saturated 1.0 M KOH solution at a scan rate of 5 mV/s. (b) Tafel plots. (c) Comparison of potentials required to reach j = 10 mA/cm^2 and Tafel slopes for all as-obtained catalysts. (d) The stability measurements of the V-CoS/Co_9S_8@CNR in 1 M KOH solution before and after 1000 cycles. All these results were collected with a 95% iR correction.

Theoretical study based on DFT calculation was employed to elucidate the performance of as-prepared catalysts with the introduction of vanadium for V-CoS/Co_9S_8@CNR. As DOS of these catalysts displayed in Figure 5f, with the continuous distribution of DOS near the Fermi level, the CoS, Co_9S_8, CoS/Co_9S_8 and V-CoS/Co_9S_8@CNR are all in metallic states with excellent electrical conductivity, the increased electronic properties of CoS/Co_9S_8 and V-CoS/Co_9S_8@CNR represented the interfacial effect of heterojunctions, facilitating the electron transfer during the reactions. Higher electrical conductivity and faster electron transport arise from the formation of V-CoS/Co_9S_8@CNR heterojunction are advantageous for the catalytic performance of OER.

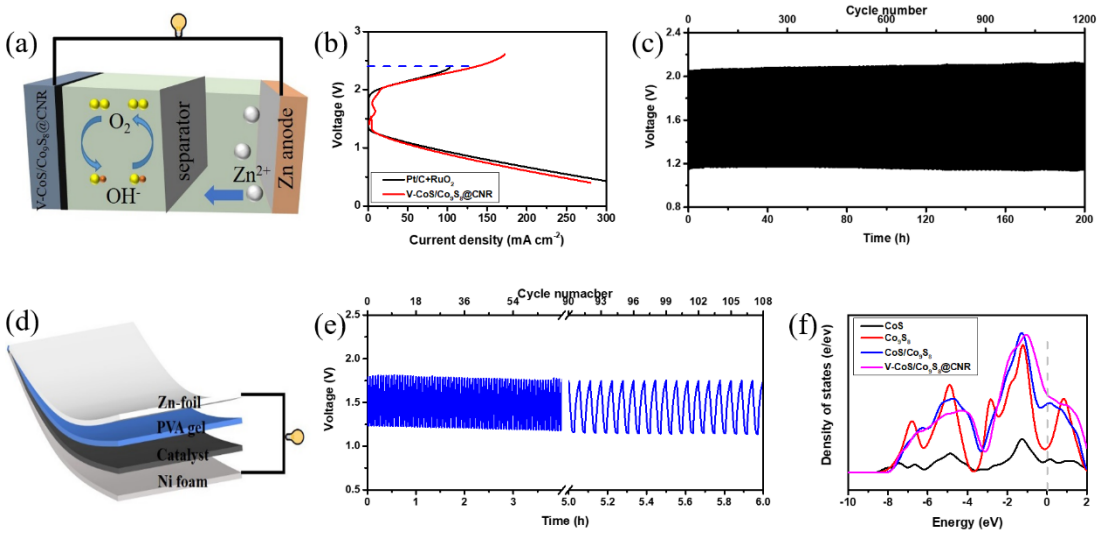

Figure 5. (a) Schematic illustration of the rechargeable Zn-air batteries. (b) Charging-discharging polarization curves. (c) cycling performance of rechargeable Zn-air batteries assembled with V-CoS/Co_9S_8@CNR electrocatalysts at 10 mA cm^{-2} (10 min/cycle). (d) Schematic illustration and photographs of the all-solid-state Zn-air battery. (e) Cycling performance of the all-solid-state ZAB using V-CoS/Co_9S_8@CNR at 1 mA cm^{-2}, where each cycle lasted 200 s. (f) DOS curves.

As a proof-of-concept, we assembled primary Zn-air batteries with V-CoS/Co_9S_8@CNR as the air-cathode catalyst (Figure 5a). Figure S11a shows that there is almost no loss in open-circuit voltage (OCV). Figure S11b shows that there is a peak power density of 121.5 mW cm^{-2}. Furthermore, the assembled rechargeable Zn-air batteries display that the battery has a charge current density of 136.8 mA cm^{-2}, higher than that of Pt/C+RuO_2, showing its good charge performance (Figure 5b). The battery

assembled with V-CoS/Co_9S_8@CNR exhibits excellent charge-discharge cycle stability up to 200 h (Figure 5c). Figure 5d shows a schematic of the all-solid-state ZAB. Figure 5e shows that there was a slight attenuation in round-trip efficiency, indicating a better recharge ability.

4 Conclusions

In summary, V-CoS/Co_9S_8@CNR was synthesized by a one-step calcination. It only requires 269 mV to reach 10 mA cm^{-2}, and exhibits a good ORR performance. Using V-CoS/Co_9S_8@CNR as the bifunctional ORR/OER electrocatalysts for the air electrode of a zinc-air battery, which exhibits up to 200 hours of cycle stability. Significantly, the results of experimental studies and DFT theoretical calculation further elucidated that higher electrical conductivity and faster electron transport arising from the formation of V-CoS/Co_9S_8@CNR heterojunction are advantageous for the catalytic performance of OER. The exceptional electrocatalytic performance benefits from the unusual synergistic charge-transfer coupling effects between the C and vanadium species, which promotes H_2O adsorption and then be converted to the O radical on the Co site by proton transfer, and the oxygen evolution on the Co^{3+} site with a higher electron cloud density by vanadium tuning. Moreover, this strategy can be readily extended to synthesize other sulfides by simply changing the metal sources.

ASSOCIATED CONTENT

Supporting Information.

Experimental section, SEM images, nitrogen absorption−desorption isotherm, elemental composition, XRD pattern, Raman spectrum, XPS, CV, RRDE, EIS AND RRDE curves, electrocatalytic properties for different samples.

AUTHOR INFORMATION

Corresponding Authors

*E-mail: tinglima@life.kyutech.ac.jp

*E-mail: liuanmin@dlut.edu.cn

Tel: +81-936956045

CRediT author statement

Huiuong Huang: Conceptualization, Writing-Original draft preparation, **Anmin Liu**: Theoretical calculation, **Qiaoling Kang**: Supervision, **Yinyu Ye**: Data Curation, **Hanlin Chen**: Data Curation, **Wei-Nien Su**: Supervision, **Tingli Ma**: Supervision, Funding acquisition, Project administration.

Notes

The authors declare no competing financial interest.

ACKNOWLEDGMENTS

Huiyong Huang gratefully acknowledges fellowships from the China Scholarship Council (CSC) (No. 202008050171). This work was supported by the Grant-in-Aid for Scientific Research (KAKENHI) program, Japan (B, Grant Number 19H02818), and the National Natural Science Foundation of China (Grant No. 51772039, 21703027, 51972293, 21902189 and 21902021), and Collaboration Program by and between Kyushu Institute of Technology and National Taiwan University of Science and Technology.

References

[1] W. Sun, F. Wang, B. Zhang, M. Zhang, V. Küpers, X. Ji, C. Theile, P. Bieker, K. Xu, M. Winter, A rechargeable zinc-air battery based on zinc peroxide chemistry, Science 371 (2021) 46-51, https://doi.org/10.1126/science.abb9554.

[2] J. Sun, D. Yang, S. Lowe, L. Zhang, Y. Wang, S. Zhao, P. Liu, Y. Wang, Z. Tang, H. Zhao, X. Yao, Sandwich-like reduced graphene oxide/carbon black/amorphous cobalt borate nanocomposites as bifunctional cathode electrocatalyst in rechargeable zinc-air batteries, Adv. Energy Mater. 8 (2018) 1801495, https://doi.org/10.1002/aenm.201801495.

[3] S. Wang, S. Chen, L. Ma, J. A. Zapien, Recent progress in cobalt-based carbon materials as oxygen electrocatalysts for zinc-air battery applications, Mater. Today Energy 20 (2021) 100659, https://doi.org/10.1016/j.mtener.2021.100659.

[4] S. Agarwal, X. Yu, A. Manthiram, A pair of metal organic framework (MOF)-derived oxygen reduction reaction (ORR) and oxygen evolution reaction (OER) catalysts for zinc-air batteries,

Mater. Today Energy 16 (2020) 100405, https://doi.org/10.1016/j.mtener.2020.100405.

[5] X. Liu, L. Jiang, Z. Zhu, S. Chen, Y. Dou, P. Liu, Y. Wang, H. Yin, Z. Tang, H. Zhao, Wet-chemistry grafted active pyridinic nitrogen sites on holey graphene edges as high performance ORR electrocatalyst for Zn-air batteries, Mater. Today Energy 11 (2019) 24-29, https://doi.org/10.1016/j.mtener.2018.10.010.

[6] X. Ren, Y. Wang, A. Liu, Z. Zhang, Q. Lv, B. Liu, Current progress and performance improvement of Pt/C catalysts for fuel cells, J. Mater. Chem. A 8 (2020) 24284-24306, https://doi.org/10.1039/D0TA08312G.

[7] X. Ren, Q. Lv, L. Liu, B. Liu, Y. Wang, A. Liu, G. Wu, Current progress of Pt and Pt-based electrocatalysts used for fuel cells, Sustain. Energy Fuels 4 (2020) 15-30, https://doi.org/10.1039/C9SE00460B.

[8] S. Li, W. Xie, Y. Song, M. Shao, Layered double hydroxide@polydopamine core–shell nanosheet arrays-derived bifunctional electrocatalyst for efficient, flexible, all-solid-state zinc-air battery, ACS Sustain. Chem. Eng. 8 (2019) 452-459, https://doi.org/10.1021/acssuschemeng.9b05754.

[9] Z. Zhang, Y. Tan, T. Zeng, L. Yu, R. Chen, N. Cheng, S. Mu, X. Sun, Tuning the dual-active sites of ZIF-67 derived porous nanomaterials for boosting oxygen catalysis and rechargeable zn-air batteries, Nano Res. 14 (2020) 2353-2362, https://doi.org/10.1007/s12274-020-3234-6.

[10] X. Feng, Q. Jiao, T. Liu, Q. Li, M. Yin, Y. Zhao, H. Li, C. Feng, W. Zhou, Facile synthesis of Co_9S_8 hollow spheres as a high-performance electrocatalyst for the oxygen evolution reaction, ACS Sustain. Chem. Eng. 6 (2017) 1863-1871, https://doi.org/10.1021/acssuschemen.7b03236.

[11] X. Hu, T. Huang, Y. Tang, G. Fu, J. M. Lee, Three-dimensional graphene-supported Ni_3Fe/Co_9S_8 composites: rational design and active for oxygen reversible electrocatalysis, ACS Appl. Mater. Interfaces 11 (2019) 4028-4036, https://doi.org/10.1021/acsami.8b19971.

[12] B. Deng, J. Liang, L. Yue, T. Li, Q. Liu, Y. Liu, S. Gao, A. A. Alshehri, K. A. Alzahrani. Y. Luo, X. Sun, CoFe-LDH nanowire arrays on graphite felt: a high-performance oxygen evolution electrocatalyst in alkaline media, Chin. Chem. Lett. https://doi.org/10.1016/j.cclet.2021.10.002.

[13] C. Ye, L. Zhang, L. Yue, B. Deng, Y. Cao, Q. Liu, Y. Luo, S. Lu, B. Zheng, X. Sun, A NiCo

LDH nanosheet array on graphite felt: an efficient 3D electrocatalyst for the oxygen evolution reaction in alkaline media, Inorg. Chem. Front. 8 (2021) 3162-3166, https://doi.org/10.1039/D1QI00428J.

[14] J. Yu, Y. Cao, Q. Liu, Y. Luo, Y. Liu, X. Shi, A. M. Asiri, T. Li, X. Sun, Co-MOF nanosheet arrays for efficient alkaline oxygen evolution electrocatalysis, ChemNanoMat 7 (2021) 906-909, https://doi.org/10.1039/D1QI00428J.

[15] J. Zhu, Z. Ren, S. Du, Y. Xie, J. Wu, H.Meng, Y. Xue, H. Fu, Co-vacancy-rich $Co_{1-x}S$ nanosheets anchored on rGO for high-efficiency oxygen evolution, Nano Res. 10 (2017) 1819-1831, https://doi.org/10.1007/s12274-017-1511-9.

[16] I. S. Amiinu, Z. Pu, D. He, H. G. R. Monestel, S. Mu, Scalable cellulose-sponsored functionalized carbon nanorods induced by cobalt for efficient overall water splitting, Carbon 137 (2018) 274-281, https://doi.org/10.1016/j.carbon.2018.05.025.

[17] S. Lu, J. Jiang, H. Yang, Y. J. Zhang, D. N. Pei, J. J. Chen, Y. Yu, Phase engineering of iron-cobalt sulfides for Zn-air and Na-ion batteries, ACS Nano 14 (2020) 10438-10451, https://doi.org/10.1021/acsnano.0c04309.

[18] B. Qiu, L. Cai, Y. Wang, X. Guo, S. Ma, Y. Zhu, Y. H. Tsang, Z. Zheng, R. Zheng, Y. Chai, Phosphorus incorporation into Co_9S_8 nanocages for highly efficient oxygen evolution catalysis, Small 15 (2019) 1904507, https://doi.org/10.1002/smll.201904507.

[19] H. Su, S. Song, S. Li, Y. Gao, L. Ge, W. Song, T. Ma, J. Liu, High-valent bimetal Ni_3S_2/Co_3S_4 induced by Cu doping for bifunctional electrocatalytic water splitting, Appl. Catal. B 293 (2021) 120225, https://doi.org/10.1016/j.apcatb.2021.120225.

[20] L. Wang, X. Duan, X. Liu, J. Gu, R. Si, Y. Qiu, Y. Qiu, D. Shi, F. Chen, X. Sun, J. Lin, J. Sun, Atomically dispersed Mo supported on metallic Co_9S_8 nanoflakes as an advanced noble-metal-free bifunctional water splitting catalyst working in universal pH conditions, Adv. Energy Mater. 10 (2019) 1903137, https://doi.org/10.1002/aenm.201903137.

[21] L. L. Wu, Q. S. Wang, J. Li, Y. Long, Y. Liu, S. Y. Song, H. J. Zhang, Co_9S_8 nanoparticles-embedded N/S-codoped carbon nanofibers derived from metal-organic framework-wrapped CdS nanowires for efficient oxygen evolution reaction, Small 14 (2018) 1704035, https://doi.org/10.1002/smll.201704035.

[22] J. Bai, T. Meng, D. Guo, S. Wang, B. Mao, M. Cao, Co_9S_8@MoS_2 core-shell heterostructures as trifunctional electrocatalysts for overall water splitting and zn-air batteries, ACS Appl. Mater. Interfaces 10 (2018) 1678-1689, https://doi.org/10.1021/acsami.7b14997.

[23] J. Long, Y. Gong, J. Lin, Metal-organic framework-derived Co_9S_8@CoS@CoO@C nanoparticles as efficient electro- and photo-catalysts for the oxygen evolution reaction, J. Mater. Chem. A 5 (2017) 10495-10509, https://doi.org/10.1039/C7TA01447C.

[24] D. Li, W. Zhang, J. Zeng, B. Gao, Y. Tang, Q. Gao, Nickel-doped Co_4N nanowire bundles as efficient electrocatalysts for oxygen evolution reaction, Sci. China Mater. 64 (2021) 1889-1899, https://doi.org/10.1007/s40843-020-1590-x.

[25] J. Zhang, X. Zhao, L. Du, Y. Li, L. Zhang, S. Liao, J. B. Goodenough, Z. Cui, Antiperovskite nitrides $CuNCo_{3-x}Vx$: highly efficient and durable electrocatalysts for the oxygen-evolution reaction, Nano Lett. 19 (2019) 7457-7463, https://doi.org/10.1021/acs.nanolett.9b03168.

[26] S. Chakrabartty, S. Karmakar, C. R. Raj, An electrocatalytically active nanoflake-like Co_9S_8-$CoSe_2$ heterostructure for overall water splitting, ACS Appl. Nano Mater. 3 (2020) 11326-11334, https://doi.org/10.1021/acs.nanolett.9b03168.

[27] S. Huang, Z. Jin, Y. Ding, P. Ning, Q. Chen, J. Fu, Q. Zhang, J. Zhang, P. Xin, Y. Jiang, Z. Hu, Encapsulating Fe_2O_3 nanotubes into carbon-coated Co_9S_8 nanocages derived from a MOFs-directed strategy for efficient oxygen evolution reactions and Li-ions storage, Small 17 (2021) 2103178, https://doi.org/10.1002/smll.202103178.

[28] T. Zhao, X. Shen, Y. Wang, R. K. Hocking, Y. Li, C. Rong, K. Dastafkan, Z. Su, C. Zhao, In situ reconstruction of V-doped Ni_2P pre-catalysts with tunable electronic structures for water oxidation, Adv. Funct. Mater. 31 (2021) 31 2100614, https://doi.org/10.1002/adfm.202100614.

[29] X. Dong, Y. Jiao, G. Yang, H. Yan, A. Wu, D. Guo, Y. Wang, C. Tian, H. Fu, One-dimensional Co_9S_8-V_3S_4 heterojunctions as bifunctional electrocatalysts for highly efficient overall water splitting, Sci. China Mater. 64 (2021) 1396-1407, https://doi.org/10.1007/s40843-020-1541-9.

[30] Z. W. Gao, T. Ma, X. M. Chen, H. Liu, L. Cui, S. Z. Qiao, J. Yang, X. W. Du, Strongly coupled CoO nanoclusters/CoFe LDHs hybrid as a synergistic catalyst for electrochemical water oxidation, Small 14 (2018) 1800195, https://doi.org/10.1002/smll.201800195.

[31] J. Sun, H. Xue, N. Guo, T. Song, Y. R. Hao, J. Sun, J. Zhang, Q. Wang, Synergetic metal defect

and surface chemical reconstruction into $NiCo_2S_4$/ZnS heterojunction to achieve outstanding oxygen evolution performance, Angew. Chem. Int. Ed. 60 (2021), 19435-19441, https://doi.org/10.1002/anie.202107731.

[32] H. Zhang, J. Wang, F. Qin, H. Liu, C. Wang, V-doped Ni_3N/Ni heterostructure with engineered interfaces as a bifunctional hydrogen electrocatalyst in alkaline solution: simultaneously improving water dissociation and hydrogen adsorption, Nano Res. 14 (2021) 3489-3496, https://doi.org/10.1007/s12274-021-3559-9.

[33] X. T. Gao, X. D. Zhu, S. R. Le, D. J. Yan, C. Y. Qu, Y. J. Feng, K. N. Sun, Y. T. Liu, Boosting high-rate lithium storage of V_2O_5 nanowires by self-assembly on N-doped graphene nanosheets, ChemElectroChem 3 (2016) 1730-1736, https://doi.org/10.1002/celc.201600305.

[34] X. Luo, Q. Zhou, S. Du, J. Li, J. Zhong, X. Deng, Y. Liu, Porous Co_9S_8/Nitrogen, sulfur-doped carbon@Mo_2C dual catalyst for efficient water splitting, ACS Appl. Mater. Interfaces 10 (2018) 22291-22302, https://doi.org/10.1021/acsami.8b06166.

[35] M. Al-Mamun, Y. Wang, P. Liu, Y. Zhong, H. Yin, X. Su, H. Zhang, H. Yang, D. Wang, Z. Tang, H. Zhao, One-step solid phase synthesis of highly efficient and robust cobalt pentlandite electrocatalyst for oxygen evolution reaction, J. Mater. Chem. A 4 (2016) 18314-18321, https://doi.org/10.1039/C6TA07962H.

[36] Y. Rao, S. Chen, Q. Yue, Y. Kang, Optimizing the spin states of mesoporous Co_3O_4 nanorods through vanadium doping for long-lasting and flexible rechargeable Zn–air batteries, ACS Catal. 11 (2021) 8097-8103, https://doi.org/10.1021/acscatal.1c01585.

[37] X. Luo, P. Ji, P. Wang, R. Cheng, D. Chen, C. Lin, J. Zhang, J. He, Z. Shi, N. Li, S. Xiao, S. Mu, Interface engineering of hierarchical branched Mo-doped Ni_3S_2/Ni_xP_y hollow heterostructure nanorods for efficient overall water splitting. Adv. Energy Mater. 10 (2020) 1903891, https://doi.org/10.1002/aenm.201903891.

[38] W. Z. Chen, P. Y. Liu, L. Zhang, Y. Liu, Z. Liu, J. He, Y. Q. Wang, High-efficient and durable overall water splitting performance by interfacial engineering of Fe-doped urchin-like Ni_2P/Ni_3S_2 heterostructure. Chem. Eng. J. 424 (2021) 130434, https://doi.org/10.1016/j.cej.2021.130434.

[39] H. Zhang, B. Xi, Y. Gu, W. Chen, S. Xiong, Interface engineering and heterometal doping Mo-

$NiS/Ni(OH)_2$ for overall water splitting, Nano Res. 14 (2021) 3466-3473, https://doi.org/10.1007/s12274-021-3557-y.

[40] Y. Zhang, B. Ouyang, J. Xu, G. Jia, S. Chen, R. S. Rawat, H. J. Fan, Rapid synthesis of cobalt nitride nanowires: highly efficient and low-cost catalysts for oxygen evolution, Angew. Chem. Int. Ed. 128 (2016) 8812-8816, https://doi.org/10.1002/ange.201604372.

[41] H. Sun, Y. Min, W. Yang, Y. Lian, L. Lin, K. Feng, Z. Deng, M. Chen, J. Zhong, L. Xu, Y. Peng, Morphological and electronic tuning of Ni_2P through iron doping toward highly efficient water splitting, ACS Catal. 9 (2019) 8882-8892, https://doi.org/10.1021/acscatal.9b02264.

[42] J. Zhang, J. Liu, L. Xi, Y. Yu, N. Chen, S. Sun, W. Wang, K. M. Lange, B. Zhang, Single-atom Au/NiFe layered double hydroxide electrocatalyst: probing the origin of activity for oxygen evolution reaction, J. Am. Chem. Soc. 140 (2018) 3876-3879, https://doi.org/10.1021/jacs.8b00752.

[43] N. Yao, P. Li, Z. Zhou, Y. Zhao, G. Cheng, S. Chen, W. Luo, Synergistically tuning water and hydrogen binding abilities over Co_4N by Cr doping for exceptional alkaline hydrogen evolution electrocatalysis, Adv. Energy Mater. 9 (2019) 1902449, https://doi.org/10.1002/aenm.201902449.